IEEE Access
Multidisciplinary | Rapid Review | Open Access Journal

Received May 27, 2020, accepted June 11, 2020, date of publication June 19, 2020, date of current version July 1, 2020.

Digital Object Identifier 10.1109/ACCESS.2020.3003798

Analysis, Modeling and Control of a Hybrid Drive Wind Turbine With Hydrogen Energy Storage System

WENLIANG YIN[1], (Member, IEEE), LIN LIU[2], AND XIAOMING RUI[3]

[1]School of Electrical and Electronic Engineering, Shandong University of Technology, Zibo 255000, China
[2]School of Electrical and Data Engineering, University of Technology Sydney, Sydney, NSW 2007, Australia
[3]School of Energy, Power and Mechanical Engineering, North China Electric Power University, Beijing 102206, China

Corresponding author: Lin Liu (lin.liu@student.uts.edu.au)

This work was supported in part by the Fundamental Research Funds for the Central Universities under Grant 2017XS064 and Grant 2017MS074.

ABSTRACT Hybrid drive wind power generation system, equipped with the speed regulating differential mechanism (SRDM), is able to be friendly connected to power grid without the need of partly- or fully-rated converters. The novel transmission schemes can promote not only the output power quality but also the low voltage ride through (LVRT) capability of the existing wind turbines (WTs). For the purpose of further improving the grid-connected operating performances of SRDM-based WT, this paper aims to develop a hybrid power production unit, in which the hydrogen storage system (HSS), comprising an electrolyzer, a hydrogen fuel cell and a supercapacitor, is integrated into SRDM-based WT. The basic architecture and numerical modelling methods of key subsystems in SRDM-based WT as well as in HSS are analyzed. After determining the eight different operating modes, a power supervision approach is synthesized for the proposed SRDM-based WT with HSS, by which the power flow management between energy sources and storage elements can be realized. Case studies are carried out in the presence of different randomly varying wind speeds and grid voltage faults. The satisfactory operating performances of the proposed wind-hydrogen hybrid system in terms of maximizing wind energy utilization, suppressing output power fluctuation and improving system continuous operating stability are verified.

INDEX TERMS Wind turbine (WT), wind power integration, speed regulating differential mechanism (SRDM), hydrogen energy storage, power supervision strategy, electrolyzer.

ABBREVIATIONS

DDSG	Direct drive synchronous generator
DFIG	Double-fed induction generator
HSS	Hydrogen storage system
LVRT	Low voltage ride through
PCIS	Planet carrier input shaft
PEMFC	Proton exchange membrane fuel cell
PGT	Planetary gear train
PMSM	Permanent magnet synchronous motor
RGSRS	Ring gear speed regulating shaft
SG	Synchronous generator
SGOS	Sun gear output shaft
SRDM	Speed regulating differential mechanism
VSCF	Variable speed constant frequency
WT	Wind turbine

The associate editor coordinating the review of this manuscript and approving it for publication was Eklas Hossain.

NOMENCLATURE

A. SRDM-BASED WT

S, R, C, P	Sun gear, ring gear, planet carrier, planet gear
k	Structure parameter of PGT
$n_{(S,R,C,P,WT)}$	Rotational speeds of S, R, C, P and wind rotor
$\omega_{(S,R,C,P)}$	Angular velocities of S, R, C, P
n_S^C, n_R^C	Rotational speeds of S and R relative to C
$J_{(S,R,C)}$	Inertias of single masses that transformed by components in SGOS, RGSRS and PCIS
$\theta_{(S,R,C)}$	Angular positions in SGOS, RGSRS and PCIS
$T_{(S,R,C)}$	Torques acting on SGOS, RGSRS and PCIS
$J_{(WT,SG,m)}$	Inertias of wind rotor, SG and PMSM

$\omega_{(WT,SG,m)}$	Angular velocities of wind rotor, SG, PMSM
$T_{(WT,SG,m)}$	Torque of wind rotor, electromagnetic torques of SG and PMSM
$B_{(WT,SG,m)}$	Damping of PCIS, SGOS and RGSRS
$J_{(1,2,3,4)}$	Equivalent inertias of shafts in Fig. 3
$J_{(CL,SH,RA)}$	Equivalent inertias of PCIS, SGOS and RGSRS
m_C, η_0	Mass of C and efficiency of gear unit
$l_{(S,R,P)}$	Radius of S, R and P
L, E, V	Lagrange function, total potential energy and total kinetic energy of transmission system
Q_C, Q_R	Generalized forces in PCIS and RGSRS

B. HSS

U_{rev}	Reversible voltage of electrolytic cell
I_{el}, T_{el}, A_{el}	Inductor current, electrode area and working temperature of electrolyzer
N_{el}	Numbers of electrolytic cells
U_{Ael}	Voltage by combining N_{el} electrolytic cells
$\eta(T_{el}, I_{el})$	Faraday efficiency
F	Faraday constant
$t_{(1,2)}$	Start and end time for hydrogen production
P_t, P_{in}	Storage pressure and internal pressure of tank
V_b, T_b	Tank volume and working temperature
$M_{\mathrm{H_2}}$	Hydrogen molar mass
f_T	Compressibility factor
E_{n}^0	Standard emf of fuel cell
$P_{\mathrm{H_2}}$, P_{O_2}, P_{H_2O}	Effective partial pressures of H_2, O_2 and H_2O
i_{fc}, T_{fc}, Z_{fc}	Current, temperature and resistance of PEMFC
i_L	Limit current of PEMFC
R_g	Gas constant
C_{sc}	Capacitance of supercapacitor
C_{Asc}	Total capacitance of supercapacitor bank
ESR	Equivalent series resistance of supercapacitor
R_{Asc}	Total resistance of supercapacitor bank
n_{1sc}	Number of capacitors connected in series
n_{2sc}	Number of series strings in parallel

C. CONTROL STRATEGY

P_{el}^*, P_{el}	Reference power and actual power consumed via electrolyzer
P_{sc}^*, P_{sc}	Reference power and actual power transmitted via supercapacitor
P_{cf}^*, P_{cf}	Reference power and actual power output by PEMFC
SC	State of charge for supercapacitor
$SC_{\min}$, $SC_{\max}$	Minimum and maximum state of charge
P_{SG}	Power generated via WT
P_{load}	Power required via load
P_{HSS}	Power transmitted via HSS
I_{el}, I_{sc}, I_{cf}	Actual currents transmitted by converters used for electrolyzer, supercapacitor and PEMFC
$K_{el,P}$, $K_{el,I}$	Proportional, integral factors of electrolyzer
$K_{sc,P}$, $K_{sc,I}$	Proportional, integral factors of supercapacitor
$K_{cf,P}$, $K_{cf,I}$	Proportional, integral factors of PEMFC

I. INTRODUCTION

Challenges of energy crisis and global environmental threats have contributed to the widespread research and investment on equipment developments and applications of renewable energy sources. Grid-connected wind power generation systems, proved to have the best commercial competitiveness so far, are developing very fast and will supply up to 20% of global electricity by 2030 [1], [2]. However, owing to the volatility and intermittency natures of wind power generation, the problems in wind energy industry in terms of increasing peak shaving complexity, reducing output power quality as well as depraving system operation stability exist. As a result, friendly grid-connected wind power consumption is hindered and severe wind electrical energy abandonment happens in many countries [3], [4].

In renewable energy market, most WTs work with the mode of variable speed constant frequency (VSCF) to shrink the impacts on power system and to improve the capacity factor of wind farms. Generally, the high-power frequency converters and accompanying complex control systems are employed to ensure that the output current frequency remains consistent with respect to the system frequency. Although these existing VSCF WTs possess a number of advantages, WTs with double-fed induction generator (DFIG) have poor low voltage ride-through (LVRT) capability, which means that the power system stability may be deteriorated if large-scale DFIGs are incorporated into power grid [5], [6]. WTs with direct drive synchronous generator (DDSG) have satisfactory LVRT capability but need fully-rated converters. The huge energy dissipation and high cost exist [7]. Moreover, in the commercially operating wind farms, harmonic pollutants can always be excited by the rectifier-inverter links of converter and then transmitted to the power grid to distort the normally smooth sinusoidal voltage [8], [9].

To effectively address these problems of existing VSCF WTs, in combination with differential gear set and hydraulic or electrical actuator devices, a series of novel alternative transmission systems were presented for grid-connected WTs by universities and institutes, in which synchronous generator (SG) can output system-frequency electricity power by using mechanical speed regulators instead of fully- or partially-rated converters. Compared with

the existing DFIG- and DDSG-based wind power systems, WTs with mechanical speed regulators are proved to have significant advantages (such as promoting the energy efficiency, improving the grid-connected operating performance and reducing the system total cost), as well as good potential for solving shortcomings in large-scale wind power utilization [10]–[26].

Taking SRDM-based WT as research object, researchers deeply studied the conceptual scheme design methods and kinematic transmission principles of this kind of WTs [10]–[14]. In these schemes, special planetary gear trains (PGTs) equipped with controllable permanent magnet synchronous motors (PMSMs) were employed to keep the generators operating stably at the rated speed. The key parameters of PMSM including timing amplifier, timing depth and timing bandwidth were calculated and the scheme availability was preliminarily verified as well. In [15]–[17], Lin, Zhao and Jelaska *et al*. analyzed the power splitting characteristics of hybrid drive WT and calculated its mechanical transmission efficiency. Case studies indicated that the overall efficiency of their proposed WT was 2.1% higher than that of the WTs with typical gearbox. Furthermore, the advanced control strategies for ensuring the desired PMSM speed regulating performance [18]–[22] and for achieving the maximal power point tracking [23], [24] were synthesized under structured and unstructured uncertainties. In [25], [26], experimental studies were demonstrated in high-power test platforms to investigate the feasibility, transient performance and power split behavior of WT based on electrically controlled SRDM.

Among these achievements, researchers have carried out significant works about the overall scheme design methods, speed regulating principles, transmission characteristics, speed control strategies as well as the feasibility analysis for this new-type WTs. However, since the original intentions for designing SRDM-based WTs are to handle the problems caused by unstable wind power integration, it is convincing that substantial works are still needed to further improve the grid-connected operating performances of SRDM-based WT. Meanwhile, developments and applications of energy storage technology have provided an effective technical approach for the friendly connection of wind power electricity to the grid. The advantages for integrating energy storage unit into wind power generation system are mainly manifested in that, the peak shaving complexity and output power fluctuations can be relieved, the undesired impacts on power grid frequency and voltage stability, aroused via wind farms, can also be mitigated [2], [27]. Meanwhile, hydrogen storage system, based on electrolyzers and hydrogen fuel cells, is considered as an ideal means for long-term energy storage. Coupled with supercapacitors, the unsought slow dynamic response of HSS can be alleviated. In this case, wind-hydrogen hybrid systems are studied worldwide for the good potential in handling the problems coming from large-scale and high-proportion wind energy injection into the power grid [28], [29].

In our previous work, a new-type SRDM-based WT was proposed to generate constant-frequency electricity without converters. The transmission characteristics and robust speed control methods of PMSM were studied, and the feasibility and superiority of SRDM-based WT were also verified [12]–[14], [21], [22]. In this paper, the harmonious combination of HSS and SRDM-based WT is successfully realized. Then, the basic architecture, power conversion mechanism as well as the numerical modelling methods of the proposed SRDM-based WT with HSS are all studied. After synthesizing the corresponding controllers for key equipment layer, a power supervision approach is proposed for SRDM-based WT with HSS under the consideration of wind speed fluctuation, load demand, hydrogen storage level and slow system dynamics. By using the proposed approach, the effective power flow management between energy sources and storage elements as well as the fast difference compensation between wind power and load during different operating modes can be guaranteed. Finally, case studies, under different wind speed conditions and gird voltage faults, are carried out via a built dedicated simulation model. The improvements of the proposed wind-hydrogen hybrid system in energy efficiency, power quality and grid-connected operating performances are all validated.

The remaining of this paper is organized as follows. Section II introduces the basic architecture and transmission principles of SRDM-based WT with HSS. The key subunit control methods as well as the energy management strategy are synthesized in Section III. In Section IV, the dedicated simulation model is developed. Moreover, the test system is utilized for the case studies to validate the effectiveness and superiority of the proposed approaches. Conclusion part is given in Section V.

II. SYSTEM DESCRIPTIONS AND METHODOLOGY

A. INTRODUCTIONS OF SRDM-BASED WT WITH HSS

In this section, detailed descriptions of the integrated system are given and numerical models of key units are established. Fig. 1 shows the basic architecture of the proposed SRDM-based WT with HSS. It can be seen that SRDM-based WT consists of the wind rotor, step-up gearbox, SRDM system, synchronous generator, transformer and power grid, while HSS is composed of the electrolyzer, air compressor, gas storage tank, proton exchange membrane fuel cell (PEMFC) and supercapacitor.

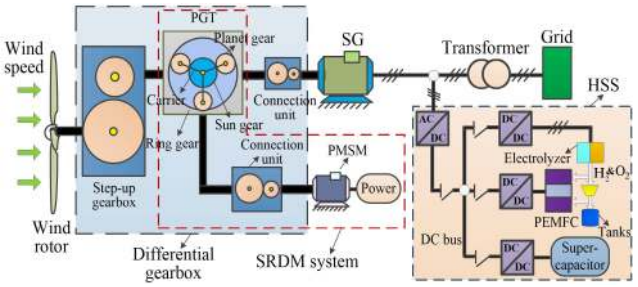

FIGURE 1. Layout of the proposed SRDM-based WT with HSS.

Here, to sustain the power demand and to solve the wind energy abandonment, when the electric power generated by WT is excessive, electrolyzer units can absorb the remaining power for electrolytic hydrogen production. The hydrogen and oxygen obtained during electrolysis process are able to be used not only for charging PEMFC, but also for industrial and medical applications. If the load demand is difficult to meet, PEMFC would perform as a generator and is able to quickly compensate for the power gap. In both the working conditions, supercapacitor always plays the role as a buffer to circumvent the slow dynamic behavior of HSS. As a result, the effects of wind power fluctuation and even the available power absence from SRDM-based WT can be effectively tackled. Moreover, when grid voltage faults occur, HSS can absorb part of instantaneous energy from SG to ensure the equipment safety. Coupled with the reactive power support function, LVRT capability of WTs is able to be improved.

B. MODELS AND DYNAMICS OF SRDM-BASED WT

1) SPEED REGULATING PRINCIPLES OF SRDM

Planetary gear train, with two degrees of freedom, is the key functional unit of SRDM system, as shown in Fig. 2. By using PGT, the dominating input from step-up gearbox can be transmitted to planet carrier while the speed regulating input generated by PMSM is delivered to ring gear. Sun gear is connected with SG directly. In order to easily obtain the speed relationships of component in PGT, the mechanical reverse method is utilized [30]. In this case, the relative speed ratio between sun gear and ring gear, marked i_{SR}^{C}, can be calculated via:

$$i_{SR}^{C} = \frac{n_S^C}{n_R^C} = \frac{n_S - n_C}{n_R - n_C} = -k \tag{1}$$

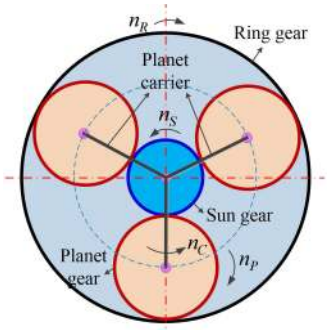

FIGURE 2. Speed relationships of planetary gear train.

Setting the transmission ratio of step-up gearbox as i_{Cw}, the speed ratio between sun gear and generator as i_{Sg}, the speed ratio between speed regulating motor (SRM) and ring gear as i_{Rm}, then the final speed ratio from wind rotor to SG, marked i_{gw}, can be derived as (2).

$$i_{gw} = \frac{n_g}{n_{WT}} = \frac{n_S}{i_{Sg} n_{WT}} = (1+k)\frac{i_{Cw}}{i_{Sg}} - k\frac{i_{Rm}}{i_{Sg}}\left(\frac{n_m}{n_{WT}}\right) \tag{2}$$

In an actual SRDM-based WT, the parameters including k, i_{Cw}, i_{Rm} and i_{Sg} are all constant. That is, i_{gw} would change with respect to the variety of n_m/n_{WT}. Therefore, if we synthesize an appropriate SRM control strategy according to (3), the SG rotational speed can be stably regulated to the rated value n_g^*.

$$n_m^* = \frac{(1+k)\, i_{Cw}}{k i_{Rm}} n_{WT} - \frac{i_{Sg}}{k i_{Rm}} n_g^* \tag{3}$$

2) DYNAMIC MODEL OF TRANSMISSION SYSTEM

By equivalently converting the kinetic parameters of SRDM internal coupling components to shafts, transmission system of SRDM-based WT can be simplified as triaxial structure, namely, planet carrier input shaft (PCIS), sun gear output shaft (SGOS) and ring gear speed regulating shaft (RGSRS), as shown in Fig. 3. We can see that the components on PCIS can be transformed as a mass with the angular displacement θ_C, the torque T_C and the total moment of inertia J_C. The same simplification process is applied to SGOS and RGSRS, as well.

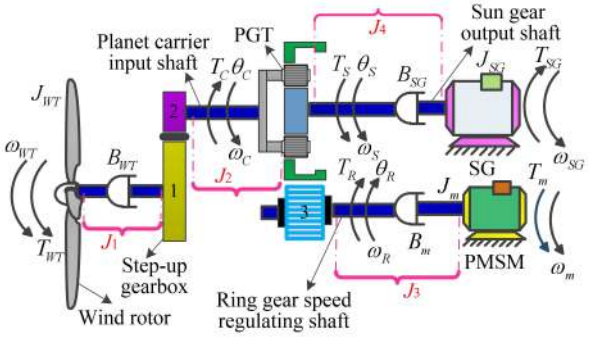

FIGURE 3. Simplified triaxial dynamic model of the proposed WT.

By utilizing the principle of inertia synthesis [31], the equivalent moments of inertia of the transformed PCIS, SGOS and RGSRS can be calculated via (4).

$$\begin{cases} J_{CL} = \dfrac{\eta_0}{i_{Cw}^2}(J_{WT} + J_1) + J_2 + m_C(l_S + l_P)^2 \\ J_{SH} = J_4 + J_{SG} \\ J_{RA} = J_m + J_3 + \dfrac{1}{\eta_0 i_{Rm}^2} J_R \end{cases} \tag{4}$$

Lagrange method [31] is used to establish the dynamic model of SRDM-based transmission system. The Lagrange function, calculated via the difference between total kinetic energy and total potential energy of system, is derived firstly.

To the author's knowledge, the elastic deformations of each shaft, gear connection unit and wind rotor, can always be neglected due to the large torsional stiffness. Thus, $V = 0$, and $L = E$ hold. After selecting the angular displacements of PCIS, SGOS and RGSRS as system generalized coordinates, the Lagrange function can be calculated by:

$$L = E = \frac{1}{2} J_{CL} \omega_C^2 + \frac{1}{2} J_{SH} \omega_S^2 + \frac{1}{2} J_{RA} \omega_R^2 + \frac{1}{2} J_P \omega_P^2 \tag{5}$$

where the system total kinetic energy (E) is composed of the rotations of wind rotor, generator, speed regulating motor and transmission shafts.

Because the proposed SRDM-based transmission has two degrees of freedom, θ_C and θ_R are chosen as the independent generalized coordinates. Additionally, we can easily get from (5) that L is only related to the generalized velocities. That is:

$$\frac{\partial L}{\partial \theta_C} \equiv 0; \quad \frac{\partial L}{\partial \theta_R} \equiv 0 \tag{6}$$

As a result, the partial derivatives of L relative to the generalized velocities can be derived as:

$$\begin{cases} \dfrac{\partial L}{\partial \dot{\theta}_C} = \dfrac{\partial L}{\partial \omega_C} = J_{CL}\omega_C + J_{SH}\omega_S \dfrac{\partial \omega_S}{\partial \omega_C} + J_P\omega_P \dfrac{\partial \omega_P}{\partial \omega_C} \\ \dfrac{\partial L}{\partial \dot{\theta}_R} = \dfrac{\partial L}{\partial \omega_R} = J_{RA}\omega_R + J_{SH}\omega_S \dfrac{\partial \omega_S}{\partial \omega_R} + J_P\omega_P \dfrac{\partial \omega_P}{\partial \omega_R} \end{cases} \tag{7}$$

In (7), two time-varying unknown parameters marked ω_S and ω_P need to be solved. According to (1), we can get that:

$$\omega_S = (1+k)\omega_C - k\omega_R \tag{8}$$

Moreover, to solve ω_P, rotational state of planetary gear is analyzed, as shown in Fig. 4. Then, the absolute velocity at point Z can therefore be calculated based on the principle of speed synthesis, as (9).

$$V_{ZY} = V_{ZX} + V_{XY} \tag{9}$$

where $V_{ZY} = l_S n_S$, $V_{XY} = (l_S + l_P)\, n_C$, $V_{ZX} = l_P n_P$.

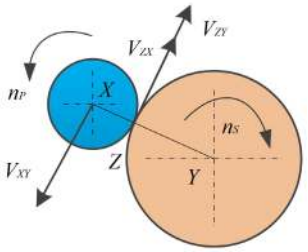

FIGURE 4. Movement status analysis of planet gear.

Combining with (8) and (9), ω_P can be obtained via:

$$\omega_P = \frac{(kl_S - l_P)\,\omega_C - kl_S\omega_R}{l_P} \tag{10}$$

Substituting ω_S and ω_P as well as $\dot{\omega}_S$ and $\dot{\omega}_P$ into (7), we can get that:

$$\begin{cases} \dfrac{\mathrm{d}}{\mathrm{d}t}\dfrac{\partial L}{\partial \dot{\theta}_C} = \left[J_{CL} + J_{SH}\,(1+k)^2 + J_P(\dfrac{kl_S - l_P}{l_P})^2\right]\dot{\omega}_C \\ \qquad - \left[k\,(1+k)\,J_{SH} + J_P(\dfrac{kl_S}{l_P} - 1)\dfrac{kl_S}{l_P}\right]\dot{\omega}_R \\ \dfrac{\mathrm{d}}{\mathrm{d}t}\dfrac{\partial L}{\partial \dot{\theta}_R} = \left[J_{RA} + k^2 J_{SH} + J_P\left(\dfrac{kl_S}{l_P}\right)^2\right]\dot{\omega}_R \\ \qquad - \left[k(1+k)J_{SH} + \dfrac{kJ_P l_S\,(kl_S - l_P)}{l_P^2}\right]\dot{\omega}_C \end{cases} \tag{11}$$

Next, Lagrange equation of the second kind is utilized to calculate the system generalized force (Q_j). Due to $V = 0$, Q_j is related only to the system virtual work done by all the non-potential forces.

According to Fig. 3, the system total virtual work can be calculated by:

$$\sum \delta W = \frac{T_{WT} - B_{WT}\omega_{WT}}{i_{Cw}}\delta\theta_C + (T_{SG} - B_{SG}\omega_S)\delta\theta_S + \frac{(T_m - B_m\omega_m)}{i_{Rm}}\delta\theta_R \tag{12}$$

In combination with the displacement constraints of PGT as (13), Q_j can thus be derived as (14).

$$\delta\theta_S l_S + \delta\theta_R l_R = (l_S + l_R)\delta\theta_C \tag{13}$$

$$\begin{cases} Q_C = \dfrac{\sum \delta W}{\delta\theta_C} = \dfrac{T_{WT} - B_{WT}\omega_{WT}}{i_{Cw}} \\ \qquad + \dfrac{(T_{SG} - B_{SG}\omega_S)\cdot(l_S + l_R)}{l_S} \\ Q_R = \dfrac{\sum \delta W}{\delta\theta_R} = \dfrac{(T_m - B_m\omega_m)}{i_{Rm}} \\ \qquad - \dfrac{L_R(T_{SG} - B_{SG}\omega_S)}{l_S} \end{cases} \tag{14}$$

By substituting (7) and (14) into the Lagrange method, the mechanical dynamic equation of SRDM-based transmission system can finally be obtained as (15).

$$\begin{bmatrix} M_1 & -M_2 \\ -M_4 & M_3 \end{bmatrix}\begin{bmatrix} \dot{\omega}_C \\ \dot{\omega}_R \end{bmatrix} = \begin{bmatrix} \dfrac{1}{i_{Cw}} & \dfrac{l_S + l_R}{l_S} & 0 \\ 0 & -\dfrac{l_R}{l_S} & \dfrac{1}{i_{Rm}} \end{bmatrix}\begin{bmatrix} T_{WT} - B_{WT}\omega_{WT} \\ T_{SG} - B_{SG}\omega_S \\ T_m - B_m\omega_m \end{bmatrix} \tag{15}$$

where

$$\begin{cases} M_1 = J_{CL} + J_{SH}\,(1+k)^2 + J_P(\dfrac{kl_S - l_P}{l_P})^2 \\ M_2 = k\,(1+k)\,J_{SH} + J_P(\dfrac{kl_S}{l_P} - 1)\dfrac{kl_S}{l_P} \\ M_3 = J_{RA} + k^2 J_{SH} + J_P\left(\dfrac{kl_S}{l_P}\right)^2 \\ M_4 = k(1+k)J_{SH} + \dfrac{kJ_P l_S\,(kl_S - l_P)}{l_P^2} \end{cases} \tag{16}$$

Equations (15) and (16) can therefore be employed to establish the numerical simulation model and to design the robust speed regulating control strategy of SRDM-based WT.

C. MATHEMATICAL MODEL OF HSS

Electrolyzer units consume the remaining wind power energy to produce hydrogen for storage or applications. Instead, once the peak time of electricity demand comes, PEMFC will provide electric power to the grid. As for a signal electrolytic

cell, the voltage at a given temperature can be calculated via Ulleberg's model as follows [29]:

$$U_{el} = U_{rev} + \frac{a_1 + a_2 T_{el}}{A_{el}} I_{el} + (b_1 + b_2 T_{el} + b_3 T_{el}^2) \times \lg(\frac{c_1 + c_2/T_{el} + c_3/T_{el}^2}{A_{el}} I_{el} + 1) \quad (17)$$

In (17), a_1 and a_2 are the Ohmic parameters of electrolyte. b_1, b_2, b_3, c_1, c_2 and c_3 are all the electrode over-voltage parameters.

Then, the total voltage by combining N_{el} electrolytic cells in series can be calculated via:

$$U_{Ael} = N_{el} U_{el} \quad (18)$$

At the same time, we use Faraday's law to calculate the hydrogen production rate of an electrolyzer cell as follows.

$$\begin{cases} N_{H2} = \eta(T_{el}, I_{el}) \dfrac{N_{el}}{2F} I_{el} \\ \eta(T_{el}, I_{el}) = d_1 \exp\left[\dfrac{d_2 + d_3 T_{el} + d_4 T_{el}^2}{(T_{el}/A_{el})} + \dfrac{d_5 + d_6 T_{el} + d_7 T_{el}^2}{(I_{el}/A_{el})^2} \right] \end{cases} \quad (19)$$

where $d_j (j = 1, 2, \cdots 7)$ are empirical parameters. The values of all electrolyzer parameters are listed in Table 1 [29].

TABLE 1. Parameters of electrolyzer.

Parameters	Values	Parameters	Values
a_1/Ω·m^2	7.33×10^{-5}	d_1/%	99.50
a_2/Ω·m^2·°C^{-1}	-1.11×10^{-7}	d_2/m^2·A^{-1}	-9.58
b_1/V	0.16	d_3/ m^2·A^{-1}·°C^{-1}	-5.55×10^{-2}
b_2/V·°C^{-1}	1.38×10^{-3}	d_4/ m^2·A^{-1}·°C^{-2}	0
b_3/V·°C^{-2}	-1.61×10^{-5}	d_5/ m^4·A^{-1}	1.50×10^3
c_1/m^2·A^{-1}	-1.60×10^{-2}	d_6/m^4·A^{-1}·°C^{-1}	-70.80
c_2/m^2·A^{-1}·°C	-1.30	d_7/ m^4·A^{-1}·°C^{-2}	0
c_3/m^2·A^{-1}·°C^2	4.12	N_{el}	360
A_{el}/m^2	0.25	T_{el}/°C	25

Thus, the total amount of hydrogen production is:

$$M_{H_2} = \int_{t_1}^{t_2} N_{H_2} dt \quad (20)$$

If PEMFC is required to provide power into the grid, the electrolyzer system would send hydrogen to it directly. The remaining amount of hydrogen need to be stored at tanks. The pressure of hydrogen tank can be obtained as [29], [32]:

$$P_t - P_{in} = f_T \frac{N_{H_2} R_g T_b}{M_{H_2} V_b} \quad (21)$$

According to the PEMFC output characteristic formula given in [32], the output voltage of a single fuel cell can be expressed as:

$$U_{fc} = E_n^0 + \frac{RT_{fc}}{2F} \ln(\frac{P_{H_2} \cdot P_{O_2}^{0.5}}{P_{H_2O}}) - \frac{RT_{fc}}{\alpha n F} \ln(\frac{i_{fc}}{i_0}) - \frac{R_g T_{fc}}{nF} \ln(1 - \frac{i}{i_L}) - iZ_{fc} \quad (22)$$

where n and a are both constant parameters.

In the designed HSS, supercapacitor bank is employed to ensure the fast dynamics of electrolyzer as well as PEMFC. By using the classical equivalent method, the supercapacitor unit model consists of a capacitance, an equivalent series resistance and a parallel resistance. In practical applications, the supercapacitor unit can be connected in series or parallel to get the desired terminal voltage and total capacitance. As a result, the total resistance and capacitance of supercapacitor bank can be calculated by (23) [33].

$$\begin{cases} R_{Asc} = n_{1sc} \dfrac{ESR}{n_{2sc}} \\ C_{Asc} = n_{2sc} \dfrac{C_{sc}}{n_{1sc}} \end{cases} \quad (23)$$

III. CONTROL STRATEGY OF SRDM-BASED WT WITH HSS

In order to guarantee the optimal power flow management of the proposed SRDM-based WT with HSS, a power supervision approach, composed of global control layer and local units control layer, is synthesized. A main controller is utilized in global control layer, by which the autonomous stable operation with the required energy measurements, decisions and controls can be realized, and then the control commands for each power units can also be produced. The local unit control layer is employed to well-track the optimal working state of subsystems.

A. GLOBAL CONTROL APPROACH

Considering the constraints of wind speed fluctuation, load demand and slow HSS dynamic response, eight different operating modes are defined.

Mode 1: If $P_{el}^* \geq P_{el}$ and $SC \leq SC_{\max}$ both hold, electrolyzer would absorb power, with the amount of P_{el}, from WT, while supercapacitor consumes the difference power, with the amount of $P_{sc}^* = P_{el}^* - P_{el}$, to alleviate power imbalance caused by electrolyzer slow dynamic response.

Mode 2: If $P_{el}^* \geq P_{el}$ and $SC > SC_{\max}$ both hold, electrolyzer absorbs power (P_{el}), while supercapacitor stops working due to the saturated charging state.

Mode 3: If $P_{el}^* < P_{el}$ and $SC > SC_{\min}$ both hold, electrolyzer absorbs power (P_{el}), while supercapacitor provides power ($P_{sc}^* = P_{el} - P_{el}^*$) to compensate for power imbalance.

Mode 4: If $P_{el}^* < P_{el}$ and $SC \leq SC_{\min}$ both hold, electrolyzer absorbs power (P_{el}), while supercapacitor stops working due to the empty charging state.

Mode 5: If $P_{fc}^* \geq P_{fc}$ and $SC \geq SC_{\min}$ both hold, PEMFC outputs power (P_{fc}) to the system, while supercapacitor also outputs power ($P_{sc}^* = P_{fc}^* - P_{fc}$) to alleviate power imbalance caused by PEMFC slow dynamic response.

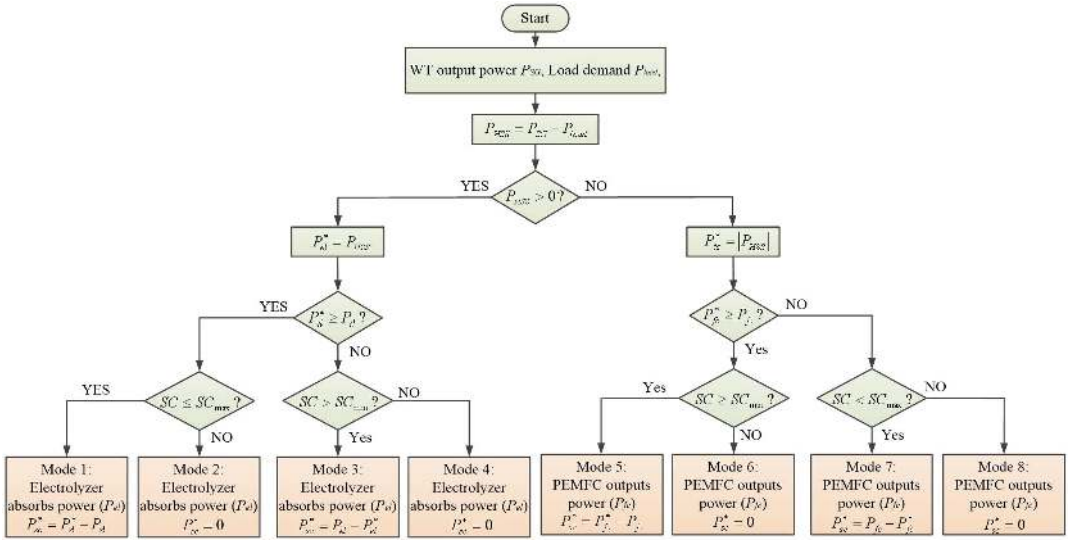

FIGURE 5. Diagram of the proposed power supervision strategy.

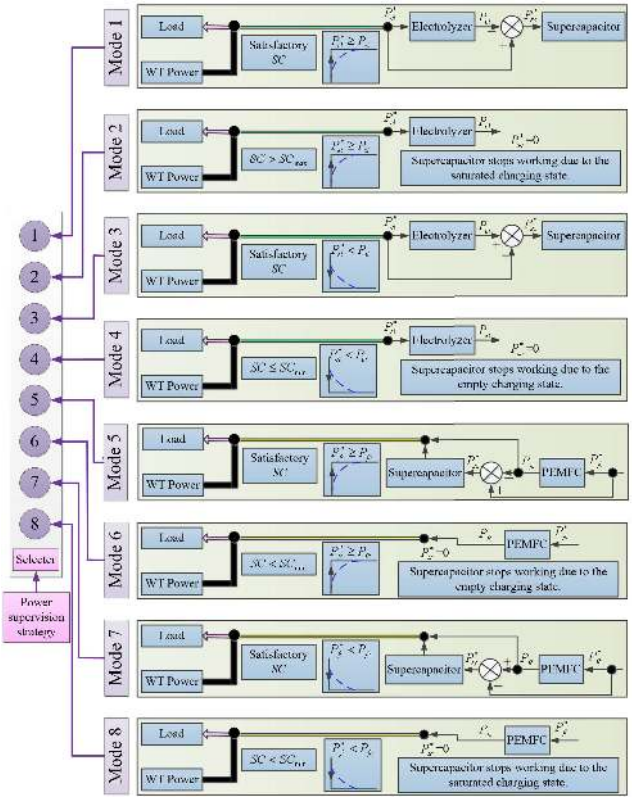

FIGURE 6. Mode selection process of the power supervision strategy.

Mode 6: If $P_{fc}^* \geq P_{fc}$ and $SC < SC_{\min}$ both hold, PEMFC outputs power (P_{fc}) to the system, while supercapacitor stops working due to the empty charging state.

Mode 7: If $P_{fc}^* < P_{fc}$ and $SC < SC_{\max}$ both hold, PEMFC outputs power (P_{fc}) to the system, while supercapacitor absorbs the difference power ($P_{sc}^* = P_{fc} - P_{fc}^*$).

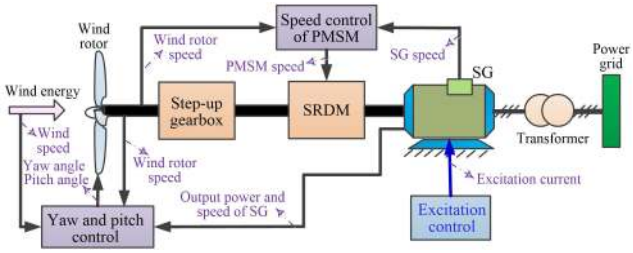

FIGURE 7. Operating principles of the proposed SRDM-based WT.

Mode 8: If $P_{fc}^* < P_{fc}$ and $SC \geq SC_{\max}$ both hold, PEMFC outputs power (P_{fc}) to the system, while supercapacitor stops working due to the saturated charging state.

Defining the power consumed/output via HSS as:

$$P_{HSS} = P_{SG} - P_{\text{load}} \tag{24}$$

As a result, the power supervision strategy is synthesized and then depicted in Fig. 5, and the detailed model selection process is illustrated as Fig. 6. Additionally, the effective control of electrolyzer, supercapacitor and PEMFC can thus be realized by the reference powers set by the designed energy flow management approach.

B. CONTROL METHODS OF KEY SUBSYSTEMS

Once the subsystems including the proposed SRDM-based WT, electrolyzer, supercapacitor and PEMFC, all receive the power control commands from main controller, local unit control layer would work to coordinate the power output via each key unit.

1) CONTROL OF SRDM-BASED WT

The operating principles of SRDM-based WT is explained as Fig. 7. It can be seen that the pitch angle, PMSM speed as well as SG excitation need to be controlled comprehensively.

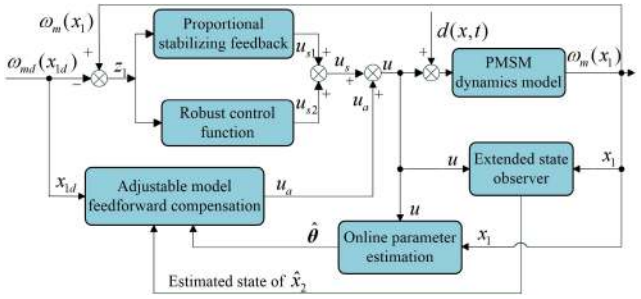

FIGURE 8. Structure diagram of PMSM speed control methods.

Researchers have done a lot of significant works about the advanced control methods of pitch angle and SG excitation. In this case, the maximum power point tracking method and the SG excitation control approach, respectively introduced in [23] and [34], are utilized.

Different from traditional VSCF WTs, SRDM-based WT is required to generate constant-frequency power without converters. That is, SG rotational speed needs to be regulated to the desired value through advanced PMSM speed control. However, the PMSM speed control accuracy can be affected seriously by parametric uncertainties and sundry external disturbances. Thus, an adaptive robust backstepping speed controller, combined with an extended state observer, is synthesized. The structure diagram of PMSM control system is given in Fig. 8 and the detailed design processes of control approach are illustrated in our previous publication [22].

2) CONTROL OF HSS

In this subsection, current single-loop PI control methods are employed. Therefore, the control equations of converters that connected with electrolyzer, supercapacitor and PEMFC can be respectively expressed as (25), (26) and (27).

$$D_{el} = (K_{el,P} + \frac{K_{el,I}}{s})(\frac{P^*_{el}}{U_{el}} - I_{el}) \tag{25}$$

$$D_{sc} = (K_{sc,P} + \frac{K_{sc,I}}{s})(\frac{P^*_{sc}}{U_{sc}} - I_{sc}) \tag{26}$$

$$D_{fc} = (K_{fc,P} + \frac{K_{fc,I}}{s})(\frac{P^*_{fc}}{U_{fc}} - I_{fc}) \tag{27}$$

The control signal of electrolyzer is obtained with the error between reference and actual currents, in which the reference current can be determined by the quotient between P^*_{el} and U_{el}. The same control process is utilized to supercapacitor and PEMFC, as well.

IV. SIMULATION MODEL AND CASE STUDIES

A. RESULTS OF NORMAL OPERATING CONDITIONS

According to the derived mathematical models as well as the designed control strategy of SRDM-based WT with HSS, a detailed 1.5 MW simulation model is developed, in which key units in regard to energy conversion, transmission system, PMSM, SG, power grid, electrolyzer, hydrogen fuel cell and control system are all simulated. In this section, the specific

TABLE 2. Parameters of the 1.5 MW simulation model.

Parameters	Values	Units
SG rated speed	1500	rpm
SG rated power	1500	kW
PMSM rated speed	3000	rpm
PMSM rated voltage	690	V
PMSM rated power	300	kW
PMSM inertia	9	kg·m^2
PMSM stator resistance	0.0149	Ω
PMSM magnet flux	0.225	Wb
Electrolyzer rated power	450	kW
Electrolyzer working temperature	25	°C
Electrolyzer working pressure	3×10^5	Pa
PEMFC rated power	400	kW
PEMFC working temperature	25	°C
Supercapacitor rated capacity	200	F
Maximum state of charge	80	%
Minimum state of charge	20	%

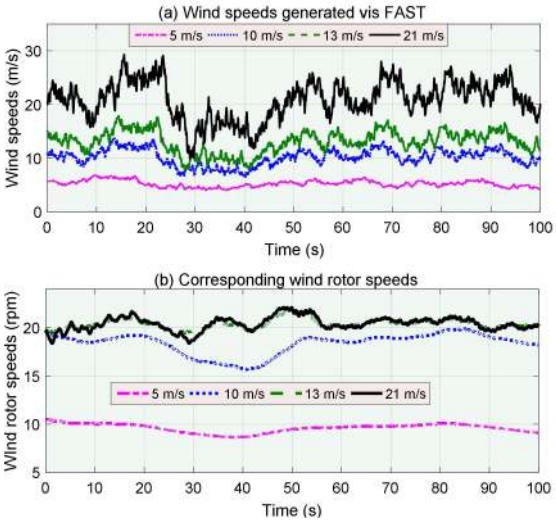

FIGURE 9. Input profiles of case studies.

speed ratios of connected pairs in drive chain are selected according to the optimization design results in [12], while the simulation module of transmission system is established based on the dynamic equations. The moments of inertia of connecting shaft are calculated via Solidworks software. The Simulink self-contained modules of PMSM, SG and power grid are utilized. Additionally, the SRDM-based WT always generates power during all the simulation period. Table 2 illustrates the vital parameters of the constructed simulation model of SRDM-based WT with HSS.

The cut in, rated and cut out wind speeds of the proposed WT are set respectively as 3 m/s, 11.7 m/s and 25 m/s. Consequently, four different cases of normal turbulent wind models (mean of 5, 10, 13, 21 m/s with 20% turbulence intensity) are generated via FAST software and employed as input profiles of case studies. Fig. 9 shows the profiles of

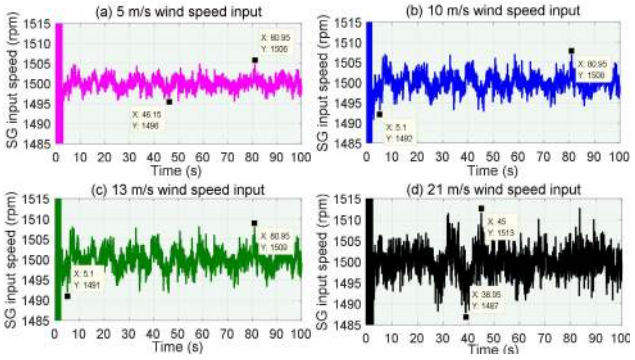

FIGURE 10. Results of SG input speeds that are adjusted to about 1500 rpm under different wind conditions.

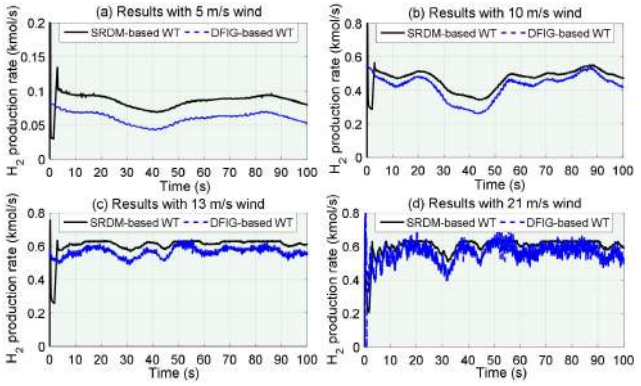

FIGURE 11. Comparative results of H_2 production rate under different wind conditions for showing the efficiency promotion performance.

changing input wind speeds and the corresponding wind rotor speeds.

SG reference rotational speed is set as 1500 rpm. In order to verify the satisfactory speed regulating ability of the proposed WT, after 100 s simulation period, SRDM output speeds that correspond directly to SG output frequency are analyzed and then expressed as Fig. 10. As shown, under four cases of wind condition, SRDM output speeds can all be kept within the range of [1485, 1515]. For 5, 10, 13, 21 m/s wind inputs, the maximum output speed errors are 0.40%, 0.53%, 0.60% and 0.87% while the average steady-state errors are 0.28%, 0.42%, 0.47% and 0.67%, respectively. Results indicate that the output power frequency of SRDM-based WT can be in accordance with the National Standard GB/T15945-2008 of P. R. China perfectly which requires the frequency average errors to be within $\pm 1\%$ and the maximum errors within $\pm 10\%$ during external disturbances.

Meanwhile, a special working mode is created to illustrate the improved system performances in terms of transmission efficiency promotion and operating economy, in which all the generated electric power of SRDM-based WT is sent to HSS for hydrogen production. Under different wind speed inputs, the comparative results about hydrogen production capacity of SRDM-based WT and existing DFIG-based WT are obtained, as shown in Fig. 11. It is obvious that the hydrogen produced via SRDM-based WT is around 5% more in amount than that of DFIG-based WT regardless of the different wind conditions. The availability and superiority of the proposed wind-hydrogen hybrid system in energy conversion efficiency are well-revealed.

By defining the load demand, grid-connected operating performances of SRDM-based WT with HSS under 21 m/s wind speed are analyzed. In this section, the proposed power supervision approach is adapted and the significant behaviors in system power balance, hydrogen balance are studied. Fig. 12 gives the simulation results of SG generated power, power flow of electrolyzer as well as PEMFC, and grid-connected power. And the hydrogen production/consumption rate are recorded as Fig. 13.

We can get from Fig. 12 that the effective power generated via SRDM-based WT can be divided among the load and

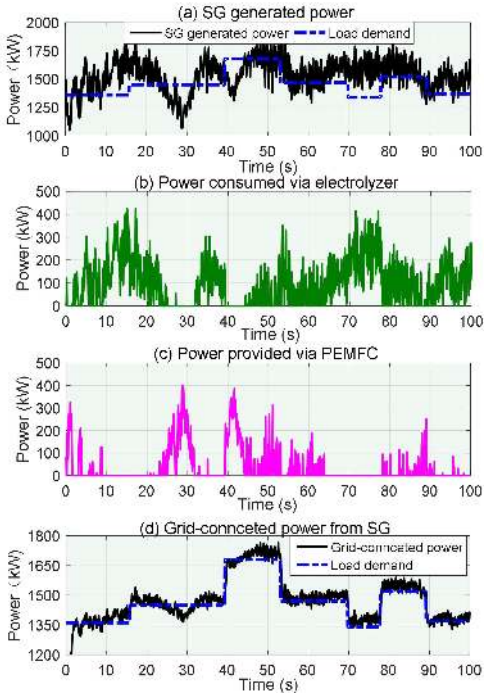

FIGURE 12. Power balance simulation results of the proposed system.

electrolyzer. On the other hand, once the WT power is unable to meet load demand, PEMFC can output power to quickly compensate for the power difference. Fig. 12 (d) shows the tracking curve of the grid-connected power respect to load demand. Compared to Fig. 12 (a), the difference power can be greatly shrunk into about 5.93% of rated power (1500 kW), while the maximum difference between SG generated power and load demand is 30.67%. Moreover, the instantly fluctuation in grid-connected power can also be effectively suppressed via HSS. The maximum steady state fluctuation of grid-connected power range at a certain load level is less than 10.41% while the maximum range of SG output power reaches 55.33%. We can also get from Fig. 13 that HSS is able to operate smoothly within the full power ranges of SRDM-based WT.

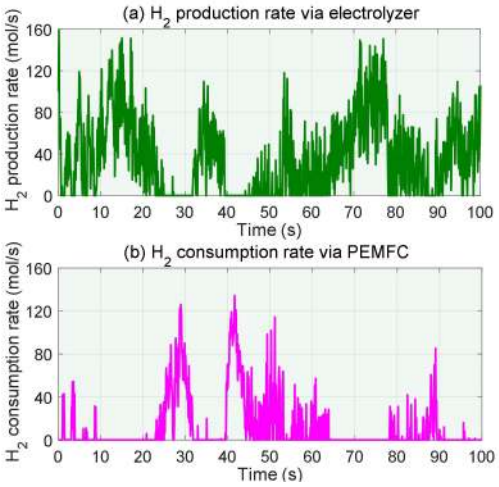

FIGURE 13. Hydrogen balance simulation results of proposed system.

B. RESULTS UNDER GRID-VOLTAGE DROP FAULTS

In this case study, the fault ride-through capability of SRDM-based WT with HSS is analyzed and then compared to that of SRDM-based WT without HSS as well as DFIG-based WT. Two different types of faults at 25 kV bus are triggered. They are case (i) (a three-phase short-circuit fault accompanied by the voltage symmetrical drop with a depth of 1 p.u. from t = 5 s to t = 5.15 s) and case (ii) (a C-type line-to-line fault accompanied by the voltage asymmetrical drop with a depth of 1 p.u. from t = 5 s to t = 5.15 s). The comparative results under case (i) and (ii) are obtained as Fig. 14 and Fig. 15, respectively, in which the signals including bus voltages, SG stator currents, electromagnetic torques and output reactive powers are all recorded.

As shown in Fig. 14, when the grid-voltage drop fault of case (i) occurs, transient stator currents and electromagnetic torques of three-types WTs oscillate in different level. But in the proposed SRDM-based WT with HSS, the oscillation peaks of above-mentioned variables can be greatly relieved in comparison with that of the remaining two WTs, and the variables' maximum shocks at voltage drop moment are less than 1.8 p.u. which amount respectively around 85% and 60% of that for SRDM-based WT without HSS and DFIG-based WT. Moreover, it is evident from Fig. 14 (d) that enough reactive power can also be provided during fault period in SRDM-based WT with / without HSS, such that the system reactive power support capacity can be guaranteed. When a fault of Case (ii) happens, the comparative results shown in Fig. 15 are generally consistent with that under Case (i). Case studies well-verify the satisfactory LVRT capability of the proposed SRDM-based WT with HSS to handle both symmetrical and asymmetrical faults.

It should be explained that SRDM-based WT without HSS also has good LVRT capability due to the outstanding ability of SG excitation, compensating for the negative sequence component, as well as providing reactive power to the grid. However, coupled with HSS, the LVRT capability

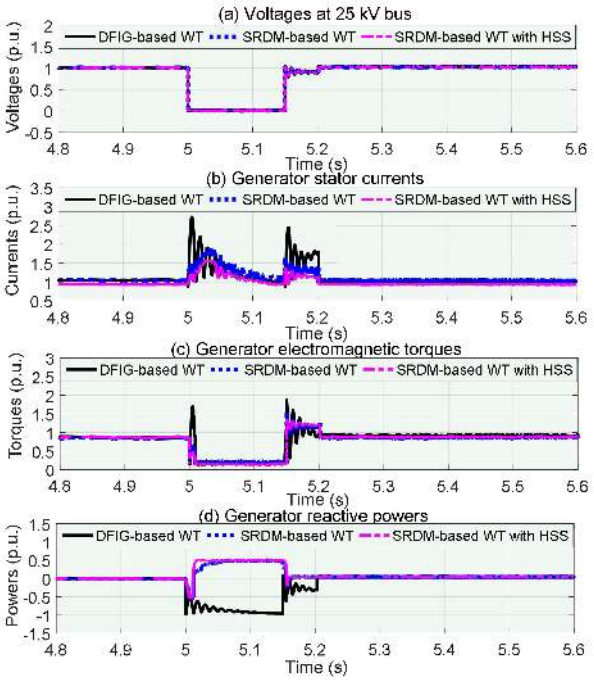

FIGURE 14. Comparative results of system LVRT capability under fault of case (i).

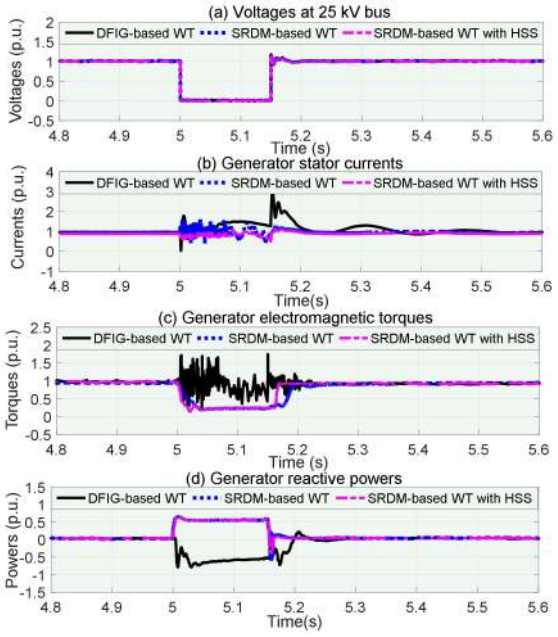

FIGURE 15. Comparative results of system LVRT capability under fault of case (ii).

of SRDM-based WT can be further improved because HSS is able to absorb instantaneous power during voltage drop period. Furthermore, the grid-connected power fluctuations in the proposed wind-hydrogen energy system can also be greatly relieved, which is helpful for improving the system continuous operating stability and thus addressing the challenges motivated by large-scale high-penetration wind power integration into power grid.

V. CONCLUSION

By applying differential speed regulation device and energy storage technology to grid-connected VSCF wind turbine, this paper proposes a basic architecture scheme of SRDM-based WT with HSS, in which SG can be utilized and connected directly to the power grid without converters. Its energy transmission principles, analyzing and numerical modelling methods as well as control strategy are deeply investigated. Case studies are carried out under different varying wind speed inputs and grid voltage faults to verify the operating feasibility and superiority of the proposed SRDM-based WT with HSS.

The main conclusions are illustrated as follows. (i) SRDM, working as a mechanical speed regulator, is able to input a stable rotate speed for SG with small errors (maximum error and average steady-state error are less than 0.87% and 0.67% respectively) that are in line with the requirements of national standard. (ii) Compared to DFIG-based WT, the hydrogen production performance of the proposed system, dominated directly by energy conversion efficiency, is promoted. About 5% more hydrogen can be obtained via SRDM-based WT no matter what the wind speed is. (iii) The application of HSS can successfully suppress the power fluctuation as well as the difference between grid-connected power and load demand (less than 5.93%) by making up or filling up the power gap, which is conducive to guaranteeing the stability of output voltage and frequency of wind farms. (iv) SRDM-based WT with HSS have satisfactory capability in terms of LVRT and reactive power production. The operating reliability of wind power generation equipment can be improved.

All the outcomes obtained in this paper can provide a convincing theoretical basis for future research and practical application of hybrid drive WT with energy storage system.

REFERENCES

[1] *Global Wind Report 2018*, Global Wind Energy Council, Istanbul, Turkey, Apr. 2019.

[2] F. Luo, K. Meng, Z. Y. Dong, Y. Zheng, Y. Chen, and K. P. Wong, "Coordinated operational planning for wind farm with battery energy storage system," *IEEE Trans. Sustain. Energy*, vol. 6, no. 1, pp. 253–262, Jan. 2015.

[3] Y. S. Sun, X. S. Tang, X. Z. Sun, D. Q. Jia, G. W. Zhang, and P. Wang, "Research on energy storage capacity allocation method for smoothing wind power fluctuations," *Proc. CSEE*, vol. 37, no. S1, pp. 88–97, Jan. 2017.

[4] J. Ouyang, M. Li, Z. Zhang, and T. Tang, "Multi-timescale active and reactive power-coordinated control of large-scale wind integrated power system for severe wind speed fluctuation," *IEEE Access*, vol. 7, pp. 51201–51210, Apr. 2019.

[5] Y. Chi, W. Liang, and Z. Zhang, "An overview on key technologies regarding power transmission and grid integration of large-scale offshore wind power," *Proc. CSEE*, vol. 36, no. 14, pp. 3758–3770, Jul. 2016.

[6] I. Ngamroo and T. Karaipoom, "Improving low-voltage ride-through performance and alleviating power fluctuation of DFIG wind turbine in DC microgrid by optimal SMES with fault current limiting function," *IEEE Trans. Appl. Supercond.*, vol. 24, no. 5, pp. 1–5, Oct. 2014.

[7] V. Yaramasu, B. Wu, S. Alepuz, and S. Kouro, "Predictive control for low-voltage ride-through enhancement of three-level-boost and NPC-converter-based PMSG wind turbine," *IEEE Trans. Ind. Electron.*, vol. 61, no. 12, pp. 6832–6843, Dec. 2014.

[8] S. Liang, Q. Hu, and W.-J. Lee, "A survey of harmonic emissions of a commercially operated wind farm," *IEEE Trans. Ind. Appl.*, vol. 48, no. 3, pp. 1115–1123, May 2012.

[9] M. Kesraoui, A. Chaib, A. Meziane, and A. Boulezaz, "Using a DFIG based wind turbine for grid current harmonics filtering," *Energy Convers. Manage.*, vol. 78, pp. 968–975, Feb. 2014.

[10] M. Idan and D. Lior, "Continuous variable speed wind turbine: Transmission concept and robust control," *Wind Eng.*, vol. 24, no. 3, pp. 151–167, May 2000.

[11] A. L. Mu, H. Z. Liu, and M. H. Zhang, "Theory and kinematic analysis of a novel variable speed constant frequency wind energy conversion system," *Chin. J. Mech. Eng.*, vol. 44, no. 1, pp. 196–204, Jan. 2008.

[12] R. Su, X. Rui, X. Wu, and Q. Yin, "The design and analysis of wind turbine based on differential speed regulation," *Proc. Inst. Mech. Eng. C, J. Mech. Eng. Sci.*, vol. 230, no. 2, pp. 221–229, Feb. 2016.

[13] W.-L. Yin, X.-M. Rui, L. Liu, and X. Hu, "Operating performance analysis on wind turbines with the speed regulating differential mechanism," *J. Renew. Sustain. Energy*, vol. 10, no. 6, Nov. 2018, Art. no. 063301.

[14] X. M. Rui and W. L. Yin, "Research on transmission performances of wind turbines with differential speed regulation," *China Mech. Eng.*, vol. 30, no. 5, pp. 1034–1040, May 2019.

[15] Y. Lin, L. Tu, H. Liu, and W. Li, "Hybrid power transmission technology in a wind turbine generation system," *IEEE/ASME Trans. Mechatronics*, vol. 20, no. 3, pp. 1218–1225, Jun. 2015.

[16] X. Zhao and P. Maißer, "A novel power splitting drive train for variable speed wind power generators," *Renew. Energy*, vol. 28, no. 13, pp. 2001–2011, Oct. 2003.

[17] D. Jelaska, S. Podrug, and M. Perkušić, "A novel hybrid transmission for variable speed wind turbines," *Renew. Energy*, vol. 83, pp. 78–84, Nov. 2015.

[18] X. Wu, Z. Ma, X. Rui, W. Yin, M. Zhang, and K. Ji, "Speed control for the continuously variable transmission in wind turbines under subsynchronous resonance," *Iranian J. Sci. Technol., Trans. Mech. Eng.*, vol. 40, no. 2, pp. 151–154, Jun. 2016.

[19] X.-X. Yin, Y.-G. Lin, and W. Li, "Operating modes and control strategy for megawatt-scale hydro-viscous transmission-based continuously variable speed wind turbines," *IEEE Trans. Sustain. Energy*, vol. 6, no. 4, pp. 1553–1564, Oct. 2015.

[20] L. Xiaoqing, D. Haiying, L. Hongwei, L. Mingxue, and S. Zhiqiang, "Optimization control of front-end speed regulation (FESR) wind turbine based on improved NSGA-II," *IEEE Access*, vol. 7, pp. 45583–45593, Apr. 2019.

[21] X. Rui, W. Yin, Y. Dong, L. Lin, and X. Wu, "Fractional-order sliding mode control for hybrid drive wind power generation system with disturbances in the grid," *Wind Energy*, vol. 22, no. 1, pp. 49–64, Jan. 2019.

[22] W. Yin, X. Wu, and X. Rui, "Adaptive robust backstepping control of the speed regulating differential mechanism for wind turbines," *IEEE Trans. Sustain. Energy*, vol. 10, no. 3, pp. 1311–1318, Jul. 2019.

[23] D. Petković, . Ćojbašić, V. Nikolić, S. Shamshirband, M. L. M. Kiah, N. B. Anuar, and A. W. Abdul Wahab, "Adaptive neuro-fuzzy maximal power extraction of wind turbine with continuously variable transmission," *Energy*, vol. 64, pp. 868–874, Jan. 2014.

[24] X.-X. Yin, Y.-G. Lin, W. Li, and H.-G. Gu, "Hydro-viscous transmission based maximum power extraction control for continuously variable speed wind turbine with enhanced efficiency," *Renew. Energy*, vol. 87, pp. 646–655, Mar. 2016.

[25] Q. Liu, R. Appunn, and K. Hameyer, "Wind turbine with mechanical power split transmission to reduce the power electronic devices: An experimental validation," *IEEE Trans. Ind. Electron.*, vol. 64, no. 11, pp. 8811–8820, Nov. 2017.

[26] D.-Y. Li, W.-C. Cai, P. Li, S. Xue, Y.-D. Song, and H.-J. Chen, "Dynamic modeling and controller design for a novel front-end speed regulation (FESR) wind turbine," *IEEE Trans. Power Electron.*, vol. 33, no. 5, pp. 4073–4087, May 2018.

[27] L. X. Fan, H. Guo, and W. Gu, "Wind power fluctuation suppression based on control coordination between energy storage and pitch angle," *Electr. Power Autom. Equip.*, vol. 36, no. 9, pp. 99–103, Sep. 2012.

[28] H. Sun, Z. Li, A. Chen, Y. Zhang, and C. Mei, "Current status and development trend of hydrogen production technology by wind power," *Trans. China Electrotechn. Soc.*, vol. 34, no. 19, pp. 4071–4083, Oct. 2019.

[29] A. Abdelkafi and L. Krichen, "Energy management optimization of a hybrid power production unit based renewable energies," *Int. J. Electr. Power Energy Syst.*, vol. 62, pp. 1–9, Nov. 2014.

[30] M. Y. Luo, *Planetary Gear Mechanism*. Beijing, China: Higher Educ. Press, 1984, pp. 13–21.
[31] R. P. Shao, *Dynamics of Mechanical Systems*. Beijing, China: Mech. Ind. Press, 2005, pp. 32–56.
[32] H. Gorgun, "Dynamic modelling of a proton exchange membrane (PEM) electrolyzer," *Int. J. Hydrogen Energy*, vol. 31, no. 1, pp. 29–38, Jan. 2006.
[33] P. Thounthong, P. Tricoli, and B. Davat, "Performance investigation of linear and nonlinear controls for a fuel cell/supercapacitor hybrid power plant," *Int. J. Electr. Power Energy Syst.*, vol. 54, pp. 454–464, Jan. 2014.
[34] A. A. Kuz'menko, "Synchronous generator nonlinear excitation system: Synergetic sliding mode control," in *Proc. Int. Siberian Conf. Control Commun. (SIBCON)*, Omsk, Russia, May 2015, pp. 1–5.

WENLIANG YIN (Member, IEEE) was born in Anhui, China, in November 1991. He received the B.Eng. degree in mechanical engineering and the Ph.D. degree in power machinery and engineering from North China Electric Power University, Beijing, China, in 2014 and 2019, respectively.

From September 2017 to September 2018, he was sponsored by the China Scholarship Council, to conduct his research at the University of New South Wales, Sydney, Australia, under the supervision of Prof. Zhao Yang Dong. He is currently a Senior Lecturer with the School of Electrical and Electronic Engineering, Shandong University of Technology, Zibo, China. His research interests include technology and equipment of wind power generation system, energy storage as well as the control and optimization of electrical equipment.

LIN LIU was born in Jilin, China, in April 1994. She received the B.Eng. degree in automation and the M.Sc. degree in control and computer engineering from North China Electric Power University, Beijing, China, in 2016 and 2019, respectively, and the M.Sc. degree in electrical engineering from South Ural State University, Chelyabinsk, Russia, in 2019. She is currently pursuing the Ph.D. degree in electrical and data engineering with the University of Technology Sydney, Sydney, Australia.

From 2017 to 2019, she was sponsored by the China Scholarship Council, to conduct her study at the South Ural State University. Her main research area includes the data analysis and mining for condition monitoring of energy and power systems and the design optimization of high-speed electrical machines.

XIAOMING RUI received the B.Eng. and M.Sc. degrees in mechanical engineering from North Eastern University, Shenyang, China, in 1979 and 1982, respectively.

He joined the School of Energy, Power and Mechanical Engineering, North China Electric Power University, Beijing, China, in 1982, and became a Full Professor, in 1991. He is currently a Ph.D. supervisor, the Director of the Mechatronic Engineering Institute, North China Electric Power University, and a Senior Member of the Chinese Mechanical Engineering Society as well as the Guiding Committee of Mechanical Engineering in universities of China. His major research interests are in the mechanical transmission theory, the technology and equipment of renewable energy systems, the optimization design of electrical equipment, and the mechanical security of overhead transmission lines impacted by wind, rain, and ice loads.